

# SPECKLE DENOISING BASED ON BIVARIATE SHRINKAGE FUNCTIONS AND DUAL-TREE COMPLEX WAVELET TRANSFORM

Shuai Xing <sup>a\*</sup>, Qing Xu <sup>a</sup>, Dongyang Ma <sup>a</sup>

<sup>a</sup>Zhengzhou Institute of Surveying and Mapping, 450052 Zhengzhou, China - xing972403@163.com

Commission I, WG I/2

**KEY WORDS:** Transformation, Algorithms, SAR, Radiometric, Processing, Image

## ABSTRACT:

Bivariate shrinkage functions (bsf) statistically denoted as joint probability density functions (pdf) and noise pdf, can be united by MAP to denoise image. Because the intensity of speckle in synthetic aperture radar (SAR) image is hypothesized to be distributed according to Rayleigh distribution, SAR image denoising modal based on bsf and dual-tree complex wavelet transform (DT-CWT) is constructed and reduced. Local variance estimation and wiener filter are used to estimate noise variance and noisy wavelet coefficients variance respectively, and they are used to choose an appreciated threshold to denoise SAR image. Experiment results demonstrate that PSNR and ENL values of denoised images are extremely larger than the speckle denoising algorithms based on discrete wavelet transform (DWT) and edge features have been perfectly preserved.

## 1. INTRODUCTION

The SAR image is produced by coherently receiving echo. Echo overlapping inevitably produced speckle noise. Speckle is a serious obstacle of SAR image object recognition and even makes some ground features disappear. (Xiao Guochao et al., 2001) So speckle has to be removed before any interpretations.

Prof. Donoho (David Donoho L., 1995) in 1995 has proposed the soft-thresholding algorithm, and proved that the filtered image  $\hat{f}^{(x)}$  could be computed by nonlinear threshold of wavelet coefficients.

But the soft-thresholding has two problems. One is that the real biorthogonal wavelet transform (RBWT) has a disadvantage, lack of shift invariance. It means that a shift of the input image can produce aliasing in the reconstructed image. (Nick Kingsbury et al., 1997) RBWT without sub-sample can produce shift invariance with huge redundancy. Prof. Nick Kingsbury (Nick Kingsbury, 1998a; Nick Kingsbury, 1998b; Peter de Rivaz et al., 2001) has developed a dual-tree algorithm with a real biorthogonal wavelet basis, and an approximate shift invariance can be obtained with limited redundancy by doubling the sampling rate at each scale, which is achieved by computing two parallel sub-sampled wavelet trees respectively. (Yi Xiang et al., 2004; Yang Mengzhao et al., 2005; Yi Xiang et al., 2005; Wang Hongxia et al., 2005) Zhang Chunhua et al. (Zhang Chunhua et al., 2005) have used soft-thresholding and hard-thresholding based on DT-CWT to despeckle SAR images, and proved DT-CWT was better than RBWT in speckle denoising.

The other problem of the soft-thresholding is that the dependences between the coefficients of two adjacent scales have been neglected. In fact they are significantly dependent, since the wavelet coefficients of child scale are derived from the parent scale. Yi Xiang et al. (Yi Xiang et al., 2005) used an interscale model to classify the coefficients into two classes: significant coefficients and insignificant coefficients. Then the former was denoised with the MAP estimator based on an intramodel, and the later was denoted as noise and set zero. But

their interscale model couldn't exactly describe the relationship of the wavelet coefficients of two adjacent scales. Wang Hongxia et al. (Wang Hongxia et al., 2005) used only one threshold to judge the dependency, which was only effective on some particular conditions. Levent S<sub>endur</sub> and Ivan W. Selesnick (Levent S<sub>endur</sub> et al., 2002a; Levent S<sub>endur</sub> et al., 2002b; Levent S<sub>endur</sub> et al., 2002c) have analyzed the dependencies between the child and parent coefficients in detail and proposed 4 models of bivariate shrinkage functions (bsf). Bsf statistically was denoted as joint probability density functions (pdf) between the wavelet coefficients of two adjacent scales, it could be united with noise pdf by MAP estimator to denoise image. And bsf have been successfully used in denoise optical images with Gaussian noise.

In this paper, speckle is hypothesized multiplicative noise according to Rayleigh distribution, and a speckle denoising modal based on bsf and DT-CWT is constructed. Section II introduces the model based on bsf in detail. The speckle denoising algorithm is described in section III. Section IV shows experiment results of 8 real SAR images and section V is conclusions.

## 2. THE SPECKLE DENOISING MODAL BASED ON BSF

Speckle is usually hypothesized a multiplicative noise

$$g = x \times n \quad (1)$$

Where  $g$  represents a real SAR image gray value,  $x$  represents an un-noised gray value,  $n$  represents speckle noise.  $n$  can be approximately described as a Rayleigh probability density function (Marc Simard et al., 1998).

The multiplicative noise can be translated to the additional noise with logarithmic transform, which can be formulated as in the wavelet domain

$$y = w + n \tag{2}$$

Here  $n$  is denoted as wavelet coefficient of noise and different with  $n$  in (1). The definition of  $n$  in the following sections is same as that in (2) without special instructions.

In (Levent S, endur et al., 2002a) the wavelet coefficient  $y_1$ ,  $w_1$ ,  $n_1$  of current scale and  $y_2$ ,  $w_2$ ,  $n_2$  at the same position of parent scale are denoted as

$$\mathbf{y} = \mathbf{w} + \mathbf{n} \tag{3}$$

where  $\mathbf{y} = (y_1, y_2)^T$ ,  $\mathbf{w} = (w_1, w_2)^T$ ,  $\mathbf{n} = (n_1, n_2)^T$ .

The problem of speckle denoising is equivalent to finding an optimal estimation  $\hat{\mathbf{w}}$  to make  $\sup_{\mathbf{x}} \|\mathbf{w} - \hat{\mathbf{w}}\|$  minimum. Then the MAP estimator  $\hat{\mathbf{w}}$  is

$$\hat{\mathbf{w}}(\mathbf{y}) = \arg \max_{\mathbf{w}} p(\mathbf{w} | \mathbf{y}) \tag{4}$$

After some manipulations and logarithmic transform, (4) can be written as

$$\hat{\mathbf{w}}(\mathbf{y}) = \arg \max_{\mathbf{w}} \{ \log [ p_{\mathbf{n}}(\mathbf{y} - \mathbf{w}) ] + \log [ p_{\mathbf{w}}(\mathbf{w}) ] \} \tag{5}$$

From this equation, in order to use this equation to estimate the original signal, we must know both pdfs of noise and original signal. We assume the joint pdf of noise as

$$P_{\mathbf{n}}(\mathbf{n}) = \frac{2n_1 n_2}{\sigma_{n1}^2 \sigma_{n2}^2} \cdot \exp \left[ - \left( \frac{n_1^2}{\sigma_{n1}^2} + \frac{n_2^2}{\sigma_{n2}^2} \right) \right] \tag{6}$$

The same problem of  $P_{\mathbf{w}}(\mathbf{w})$  appears. Levent S, endur and Ivan W. Selesnick (Levent S, endur et al., 2002a) have used the joint empirical coefficient-parent histogram to observe  $P_{\mathbf{w}}(\mathbf{w})$ . Since SAR image is a description of natural scene, we hypothesize  $P_{\mathbf{w}}(\mathbf{w})$  of SAR image is according to this distribution. Levent S, endur and Ivan W. Selesnick (Levent S, endur et al., 2002a) have proposed four models. The model 2, 3, 4 are better than model 1 but too complicated to be solved, so that we choose model 1 to estimate  $P_{\mathbf{w}}(\mathbf{w})$ .

Model 1 in (Levent S, endur et al., 2002a) is denoted as

$$p_{\mathbf{w}}(\mathbf{w}) = \frac{3}{2\pi\sigma^2} \cdot \exp \left( - \frac{\sqrt{3}}{\sigma} \cdot \sqrt{(w_1)^2 + (w_2)^2} \right) \tag{7}$$

By using logarithmic transforms of (6) and (7), (5) can be written as

$$\hat{\mathbf{w}}(\mathbf{y}) = \arg \max_{\hat{\mathbf{w}}} \left\{ - \frac{(y_1 - \hat{w}_1)^2}{\sigma_{n1}^2} - \frac{(y_2 - \hat{w}_2)^2}{\sigma_{n2}^2} + \right.$$

$$\left. \log [ 2(y_1 - \hat{w}_1)(y_2 - \hat{w}_2) ] - \frac{\sqrt{3}}{\sigma} \cdot \sqrt{(\hat{w}_1)^2 + (\hat{w}_2)^2} + f(\sigma_{n1}, \sigma_{n2}) \right\} \tag{8}$$

where  $f(\sigma_{n1}, \sigma_{n2}) = \log 3 - \log(\sigma_{n1}^2 \sigma_{n2}^2) - \log(2\pi\sigma^2)$ .

(8) is equivalent to solving the following equations together, if  $P_{\mathbf{w}}(\mathbf{w})$  is assumed to be strictly convex and differentiable:

$$\begin{aligned} \frac{2(y_1 - \hat{w}_1)}{\sigma_{n1}^2} - \frac{1}{y_1 - \hat{w}_1} - \frac{\sqrt{3}}{\sigma} \cdot \frac{\hat{w}_1}{\sqrt{\hat{w}_1^2 + \hat{w}_2^2}} &= 0 \\ \frac{2(y_2 - \hat{w}_2)}{\sigma_{n2}^2} - \frac{1}{y_2 - \hat{w}_2} - \frac{\sqrt{3}}{\sigma} \cdot \frac{\hat{w}_2}{\sqrt{\hat{w}_1^2 + \hat{w}_2^2}} &= 0 \end{aligned} \tag{9}$$

This is a bivariate equation about  $\hat{w}_1$  and  $\hat{w}_2$ , and it is hard to be solved in program and have to be deduced.

Here a new joint pdf of noise similar with (6) is denoted as

$$P_{\mathbf{n}}(\mathbf{n}) = \frac{2K}{\sigma_{n1}^2 \sigma_{n2}^2} \cdot \exp \left[ - \left( \frac{n_1^2}{\sigma_{n1}^2} + \frac{n_2^2}{\sigma_{n2}^2} \right) \right] \tag{10}$$

The difference between (6) and (10) is  $K$ . Many experiments show that when  $n_1$  and  $n_2$  are changing in  $[0, 1]$ ,  $n_1 n_2$  in (6) can be substituted by  $K$ . Figure 1 shows the surface of (6) and (10) with  $K=33$  in  $[0, 1]$ . And we find that  $K$  is a constant while the variance of  $\hat{\mathbf{w}}$  in  $[0, 255]$ . When the wavelet coefficients are normalized in  $[0, 1]$ , (10) can be substituted for (6). Then (9) can be written as

$$\begin{aligned} \frac{2(y_1 - \hat{w}_1)}{\sigma_{n1}^2} - \frac{\sqrt{3}}{\sigma} \cdot \frac{\hat{w}_1}{\sqrt{\hat{w}_1^2 + \hat{w}_2^2}} &= 0 \\ \frac{2(y_2 - \hat{w}_2)}{\sigma_{n2}^2} - \frac{\sqrt{3}}{\sigma} \cdot \frac{\hat{w}_2}{\sqrt{\hat{w}_1^2 + \hat{w}_2^2}} &= 0 \end{aligned} \tag{11}$$

After some manipulations, this equation can be written as

$$\begin{aligned} \hat{w}_1 \cdot \left( 1 + \frac{\sqrt{3} \cdot \sigma_{n1}^2}{2\sigma \cdot r} \right) &= y_1 \\ \hat{w}_2 \cdot \left( 1 + \frac{\sqrt{3} \cdot \sigma_{n2}^2}{2\sigma \cdot r} \right) &= y_2 \end{aligned} \tag{12}$$

where  $r = \sqrt{\hat{w}_1^2 + \hat{w}_2^2}$ .

We hypothesize  $\sigma_{n1} = \sigma_{n2} = \sigma_n$  and  $r$  can be written as

$$r = \left( \sqrt{y_1^2 + y_2^2} - \frac{\sqrt{3}\sigma_n^2}{2\sigma} \right)_+$$

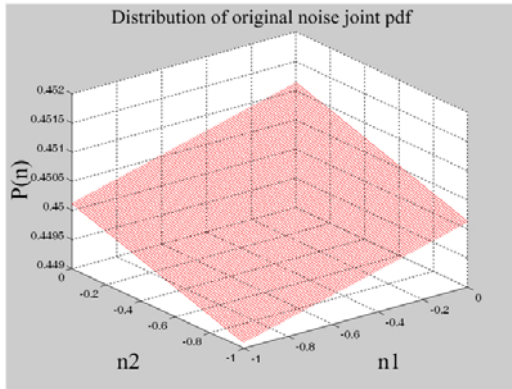
Using this in (12) then

$$\hat{w}_1 = \frac{(\sqrt{y_1^2 + y_2^2} - \frac{\sqrt{3}\sigma_n^2}{2\sigma})_+}{\sqrt{y_1^2 + y_2^2}} \cdot y_1 \quad (13)$$

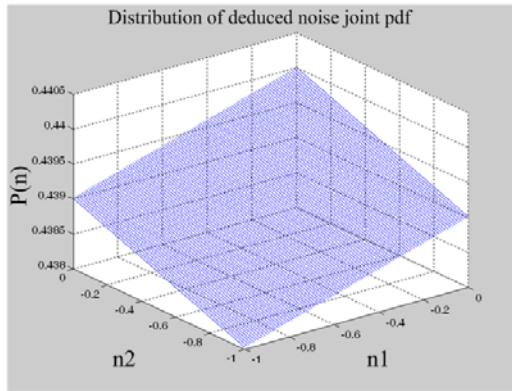
The corresponding deadzone is

$$deazone = \left\{ (y_1, y_2) : \sqrt{y_1^2 + y_2^2} \leq \frac{\sqrt{3}\sigma_n^2}{2\sigma} \right\}$$

The wavelet coefficients in deadzone are considered noise and set zero, while the wavelet coefficients out of deadzone are considered noisy signal and processed with the threshold  $\frac{\sqrt{3}\sigma_n^2}{2\sigma}$ .



(a)



(b)

Figure 1. (a). Distribution of equation (6), (b). Distribution of equation (10)

### 3. THE SPECKLE DENOISING ALGORITHM

In Figure 2 the speckle denoising algorithm based on bsf and DT-CWT includes six steps:

- 1) Logarithmic transform of the SAR image is decomposed with DT-CWT, the number of scales  $j$  usually is 5 or 6;
- 2) Normalization of the wavelet coefficients;

- 3) Compute the noise variance estimation  $\hat{\sigma}_n$  and un-noisy wavelet coefficient variance estimation  $\hat{\sigma}_i$  at scale  $j$ ;
- 4) Achieve  $\hat{w}_j$  with (13);
- 5) Restore original gray values of  $\hat{w}_j$ ;
- 6) Reconstruct and exponential transform the denoised image.

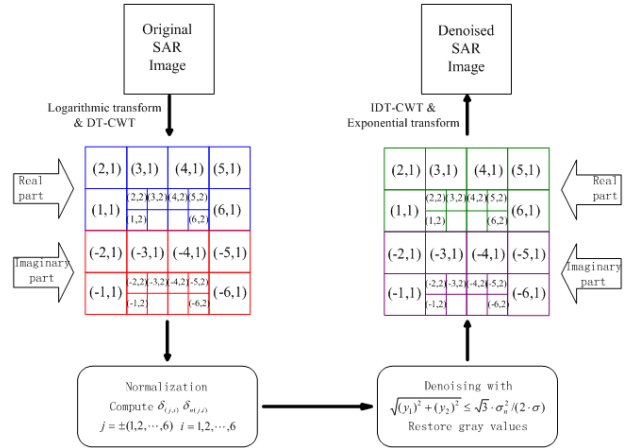


Figure 2. Flowchart of the speckle de-noising algorithm

In step 3, noise variance estimation can be computed with the method proposed by Donoho. (David Donoho L., 1995) Levent S<sub>endur</sub> and Ivan W. Selesnick (Levent S<sub>endur</sub> et al., 2002b) have denoted the relationship among noise variance  $\sigma_n$ , noise-free wavelet coefficient variance  $\sigma_w$  and wavelet coefficient variance  $\sigma_y$  was  $\sigma_y^2 = \sigma_w^2 + \sigma_n^2$ . Then the estimation of  $\sigma_w$  was  $\hat{\sigma}_w = \sqrt{\hat{\sigma}_y^2 - \hat{\sigma}_n^2}$ . In (Levent S<sub>endur</sub> et al., 2002b)  $\hat{\sigma}_y^2$  was computed by mean filter. Here we use the optimal wiener filter to achieve more accurate value.

### 4. EXPERIMENT

We choose eight real SAR images including airborne SAR, Radarsat-1, ERS-1 and ERS-2 satellite images. Speckle noise in these images is obvious. These images are shown in figure 3.

Since bivariate shrinkage models have been proved superior to the soft thresholding in (Levent S<sub>endur</sub> et al., 2002a; Levent S<sub>endur</sub> et al., 2002b; Levent S<sub>endur</sub> et al., 2002c), in this section, the proposed algorithm is only compared with the results in (Levent S<sub>endur</sub> et al., 2002a). We use two criterions, PSNR and ENL, to compare the results quantitatively. Furthermore, canny edge detector has been used to compare the ability of different algorithms to conserve edges feature of denoised images.

PSNR and ENL can represent how smooth is the de-noised image and how much noise are filtered. Higher are PSNR and ENL, smoother is the denoised image. The statistical results of 8 images are shown in Table 1. Most of PSNR and ENL of images denoised by the proposed algorithm are higher than (Levent S<sub>endur</sub> et al., 2002a). And the detailed results of Radarsat-1 image are shown in figure 4. Obviously in sight much more speckle is removed in figure 4 (d) and (e), but edges feature in figure 4 (e) are smoother and continuous.

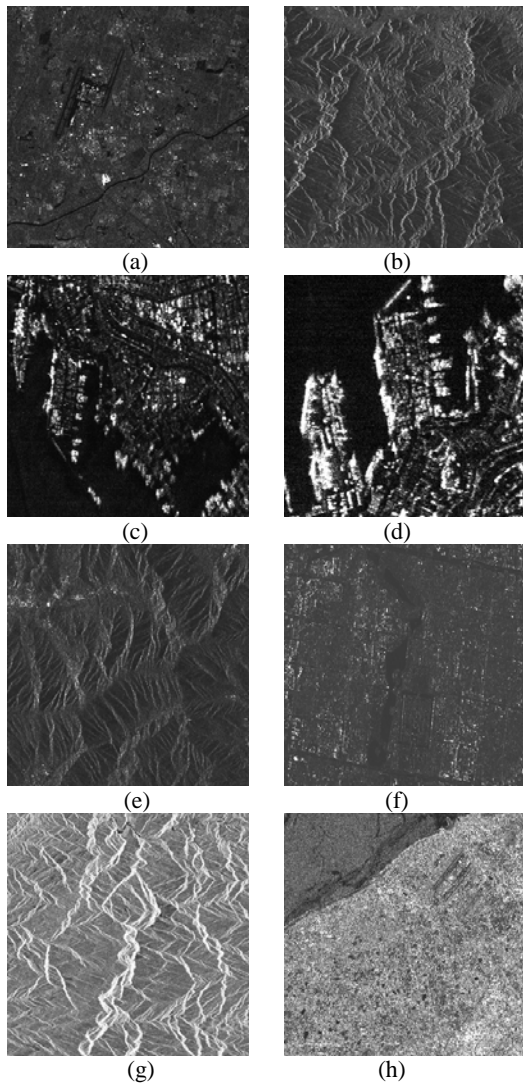


Figure 3. 8 real SAR images: (a) and (b) are ERS-2 satellite images; (c) and (d) are airborne SAR images; (e) and (f) are Radarsat-1 satellite images; (g) and (h) are ERS-1 satellite images

Radarsat-1 image and all denoised images have been detected by the Canny operator. The edge features corresponding to figure 4 are shown in figure 5. We find that mountain ridges in figure 5 (e) are continuous and easy to recognize. Especially at the top-right in figure 5 (e) more false edges have been eliminated. It will be easy to match two SAR images.

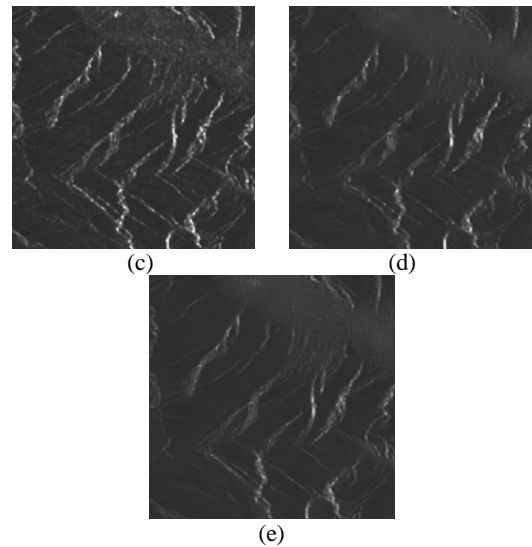
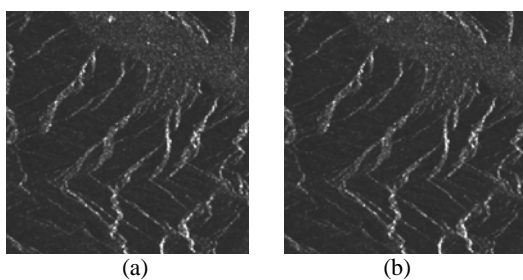


Figure 4. Partial experiment results of figure 3 (b): (a) original image; (b) image de-noised by bsf with DWT in (Levent S<sub>endur</sub> et al., 2002a); (c) image de-noised by bsf with DT-CWT in (Levent S<sub>endur</sub> et al., 2002a); (d) image de-noised by the proposed algorithm with DWT; (e) image de-noised by the proposed algorithm with DT-CWT

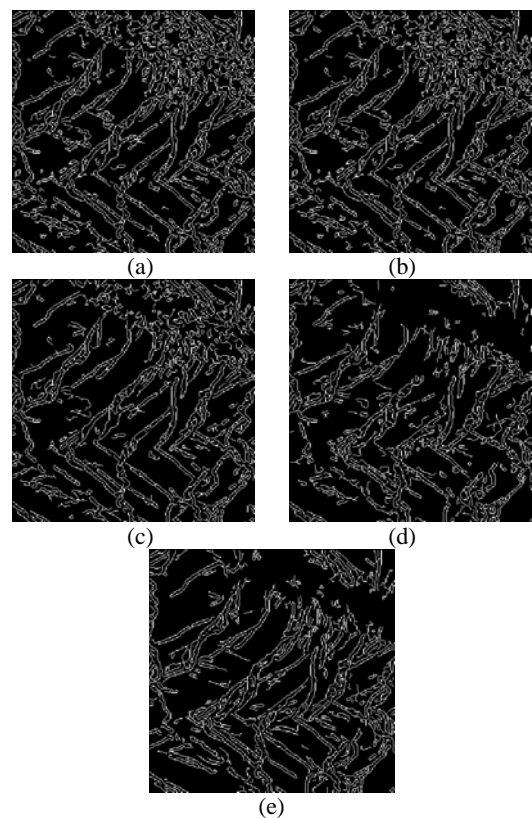


Figure 5. Edges feature of figure 4: (a) original image; (b) image de-noised by bsf with DWT in (Levent S<sub>endur</sub> et al., 2002a); (c) image de-noised by bsf with DT-CWT in (Levent S<sub>endur</sub> et al., 2002a); (d) image de-noised by the proposed algorithm with DWT; (e) image de-noised by the proposed algorithm with DT-CWT

## 5. CONCLUSIONS

In this paper, we have analyzed the principle and distribution model of speckle and proposed a speckle denoising algorithm based on bsf and DT-CWT. The bsf is used to induce the model of the dependencies of wavelet coefficients of the adjacent scales, and the noise joint pdf is reduced. Local variance estimation and wiener filter are used to estimate the filtered image. Experiment results with real SAR images have shown that much more speckle is removed and edges feature of de-noised images keep smooth and continuous. But four bsf models in (Levent S, endur et al., 2002a) are designed for optical images. The definition of the bsf model for SAR images is the future work.

**REFERENCES**

David Donoho L, 1995. De-noising by soft-thresholding, IEEE Transactions on Information Theory, 41, pp. 613-627.

Levent S, endur and Ivan W. Selesnick, 2002a. Bivariate shrinkage functions for wavelet-based denoising exploiting interscale dependency, IEEE Transactions on Signal Processing, 50(11), pp. 2744-2756

Levent S, endur and Ivan W. Selesnick, 2002b. A bivariate shrinkage function for wavelet-based denoising, Proceedings of IEEE International Conference of Acoustics, Speech, and Signal Processing. 2, pp. 1261-1264.

Levent S, endur and Ivan W. Selesnick, 2002c. Bivariate shrinkage with local variance estimation, IEEE Signal Processing Letters, 9(12), pp. 438-441.

Marc Simard, Gianfranco DeGrandi, Keith P. B. Thomson, and Goze B. B'eni'e, 1998. Analysis of speckle noise contribution on wavelet decomposition of SAR images, IEEE Transactions on Geoscience and Remote Sensing, 36(6), pp. 1953-1962.

Nick Kingsbury and Julian Magarey, 1997. Wavelet transforms in image processing, Proc. First European Conference on Signal Analysis and Prediction, Prague, pp. 23-34

Nick Kingsbury, 1998a. The dual-tree complex wavelet transform: a new technique for shift-invariance and directional filters, in DSP Workshop

Nick Kingsbury, 1998b. The dual-tree complex wavelet transform: a new efficient tool for image restoration and enhancement, Proc. European Signal Processing Conference, EUSIPCO 98, Rhodes, pp. 319-322.

Peter de Rivaz and Nick Kingsbury, 2001. Bayesian image de-convolution and de-noising using complex wavelets, Proc. IEEE Conf. on Image Processing, Greece, paper 2639

Wang Hongxia, Cheng Lizhi and Wu Yi, 2005. A complex wavelet based spatially adaptive method for noised image enhancement, Journal of Computer Aided Design & Computer Graphics, 17(9), pp. 1911-1916.

Xiao Guochao, Zhu Caiying, 2001. Radar Photogrammetry, Earthquake Press, Beijing. Pp.56-58

Yang Mengzhao, Li Chaofeng and Xu Lei, 2005. Image denosing based on complex wavelet transform and H-Curve criterion, Computer Applications, 25(4), pp. 769-774.

Yi Xiang and Wang Wei-ran, 2004. The application of statistic model for complex wavelet coefficients in image denoising, Opto-Electronic Engineering, 31(8), pp. 69-72.

Yi Xiang and Wang Weiran, 2005. A probability model for adaptive image denoising, Acta Electronica Sinica, 33(1), pp. 63-66.

Zhang Chunhua, Xu Suqin, Tao Ronghua and Chen Biao, 2005. Analysis of speckle reduction of sar images based on 2D complex wavelet, Journal of Institute of Surveying and Mapping, 22(4), pp.269-271.

	Original image		Image denoised by bsf with DWT in (Levent S, endur et al., 2002a)		Image denoised by bsf with DT-CWT in (Levent S, endur et al., 2002a)		Image denoised by bsf with DWT in this paper		Image denoised by bsf with DT-CWT in this paper	
	PNSR	ENL	PNSR	ENL	PNSR	ENL	PNSR	ENL	PNSR	ENL
Figure 3 (a)	12.8174	7.3667	12.8559	7.492	13.0292	8.3072	13.3294	12.5415	13.432	20.501
Figure 3 (b)	11.3375	3.8817	11.3812	3.9887	11.5758	4.5674	12.2223	8.8573	12.3557	14.8015
Figure 3 (c)	10.2375	0.40142	10.9974	0.48088	11.0751	0.48205	11.7579	0.79368	12.2304	1.3207
Figure 3 (d)	7.8752	0.17839	8.0492	0.18679	8.2887	0.18828	9.218	0.25724	9.7728	0.29422
Figure 3 (e)	3.4502	45.594	3.6175	101.9069	3.6309	264.2059	3.7994	218.1747	3.7732	509.6754
Figure 3 (f)	3.7318	1.8667	3.9239	3.2425	3.9489	7.5523	4.0607	6.3549	4.05	22.146
Figure 3 (g)	31.3577	34.938	32.8672	34.2168	33.6336	34.0187	33.5806	49.7928	33.8201	57.7728
Figure 3 (h)	23.6098	80.8072	25.2745	138.3005	26.801	151.9933	26.6296	257.5009	27.6259	300.5978

Table 1. Statistics of PNSR and ENL of figure 3

